Electrochemical determination of L-Cysteine by an elbow shaped, Sb-doped ZnO nanowire-modified electrode

Mashkoor Ahmad, Caofeng Pan and Jing Zhu*

Received 15th April 2010, Accepted 6th May 2010
DOI: 10.1039/c0jm01055c

Elbow shaped Sb-doped ZnO nanowires (SZO NWs) have been synthesized *via* thermal evaporation and thoroughly characterized. A glassy carbon (GC) electrode was modified by these NWs for the determination of L-cystein (L-CySH). Detailed electrochemical measurements of the modified electrode towards L- CySH oxidation are investigated. The response current of L-CySH oxidation at the SZO/GC electrode is found to be much higher than that of the bare GC and ZnO/GC electrodes. This change in the electrochemical properties of the modified electrode is due to the reduction in band gap and an increased amount of deep-level defects in SZO NWs, which leads to a significant role in the L-CySH determination. The modified electrode exhibits a reproducible sensitivity of 400 nA μM^{-1}, within a response time of less than 6s, a detection limit of 0.025 μM and a linear range of 0.075 to 100 μM. Furthermore, the modified electrode shows high stability and good resistance to interference. Our investigation demonstrates that SZO NWs are very sensitive to L-CySH and can be employed in the development of biosensors for future biological and medical applications.

1. Introduction

The study of thiols (*e.g.*, homocystein, L-cysteine, and glutathione) provides critical insight into the proper physicological function and diagnosis of disease states. This is because thiol compounds are of special significance in biochemistry and environmental chemistry.[1,2] L-Cysteine (L-CySH), due to its crucial role in biological systems, has been the subject of many electrochemical studies investigating both mechanism and detection aspects.[3] L-CySH as a thiol plays an important role in the cross linking of proteins. It has several pharmaceutical applications; namely, it is used in some antibiotics for the treatment of skin damage,[4] and as a radioprotective agent.[5] Also, it is widely used in the food industry as an antioxidant and in the pharmaceutical industry in drug formulation and as a biomarker.[6] Therefore, measuring L-CySH in body fluids, pharmaceuticals, and food samples is very important and a great deal of effort has been expended developing sensitive methods for its detection.[7] Numerous chemical and instrumental techniques for the detection of L-CySH have been reported.[8,9] In the past, electrochemical methods have been the most favored methods for the determination of thiols (particular L-cystein).[10] However, the electrochemical method for analysis of thiols remains very challenging. For example, at the conventional electrodes (*e.g.*, glassy carbon and gold electrodes), the electrochemical response of thiols is not satisfactory due to their sluggish electrochemical processes.[11–13] High overpotentials of electrochemical oxidation are needed for thiols at the conventional electrodes. This results in surface oxide formation and fouling of these electrodes.[14] In order to overcome these drawbacks, many strategies have been employed. These strategies include the use of mercury electrodes, diamond electrodes,[15,16] enzyme-based biosensors,[17] and chemically modified electrodes.[18,19] Although the analysis of thiols has improved greatly, there are still some disadvantages that hinder thiol detection. These challenges include low sensitivity, complexity and expense. Considering all this, it is critical to find a suitable material for the effective and simple determination of thiols.

The unique and fascinating properties of novel nanomaterials have triggered tremendous motivation among scientists to explore the possibilities of using them in the processes of developing new nanoscale devices for future industrial, biological, medical and bioelectronics applications.[20] Among nanomaterials ZnO, a wide band gap semiconductor, has attracted much attention due to its wide range of applications.[21–23] ZnO nanostructures exhibit interesting properties including high catalytic efficiency, catalyst support, and strong adsorption ability. Recently, ZnO has been considered as a promising material for biosensor applications because of its high isoelectric point (9.5), biocompatibility, and abundance in nature.[24] Furthermore, its nontoxicity, high chemical stability, and high electron transfer capability make ZnO a favorable material for developing implantable biosensors.[25,26] On the other hand, doping in ZnO[27] offers an effective approach to enhance the optical, electrical and electrochemical properties of nanostructures, which is crucial for their practical applications. Recently, Sb has been considered as a promising p-type dopant to enhance the ZnO properties.[28] In recent years, novel nanomaterials have been prepared to improve the electrochemical properties.[29,30] In this paper, the electroanalysis of L-cysteine at a SZO/GC modified electrode is investigated.

Beijing National Center for Electron Microscopy, The State Key Laboratory of New Ceramics and Fine Processing, Laboratory of Advanced Material, China Iron & Steel Research Institute Group, Department of Material Science and Engineering, Tsinghua University, Beijing, 100084, China. E-mail: Jzhu@mail.tsinghua.edu.cn; Fax: +861062771160; Tel: +861062794026

2. Experimental section

2.1. Reagents

Sb_2O_3 (99.998%, Aldrich) and metallic Zn powder (99.998%) were supplied by Sinopharm Chemical Regent Co. Ltd. Glucose, cholesterol, L-cysteine and uric acid were purchased from Sigma-Aldrich (Shanghai) Trading Co., Ltd. 2-propanol (99.9%) was obtained from Beijing Modern Eastern Fine Chemical. Nafion (5 wt%) was purchased from Dupont. Other chemicals were of analytical-reagent grade without further purification. All solutions in the testing were prepared using deionized water.

2.2. Controlled synthesis of undoped and Sb-doped NWs

Controlled synthesis of un-doped and Sb-doped ZnO NWs were carried out in a horizontal quartz tube furnace *via* a thermal evaporation method, where the temperature, pressure and flow rates of the working gases were well controlled. In this process, a crucible containing the mixture of Sb_2O_3 (99.998%, Aldrich) and metallic Zn powder (1 : 2 atomic ratio) was placed in the central region of the quartz tube furnace. Mixed gases (90% Ar, 10% O_2) flowed through the quartz tube at a rate of 180 sccm. The furnace temperature was increased to a designated temperature of 800 °C at a speed of 10 deg min^{-1} for 3 h. A Si substrate, after being cleaned carefully for 30 min, is mounted downward of the furnace where the temperature was 550 °C. Two samples with or without Sb doping were prepared under the same conditions.

2.3. Apparatus

The as-prepared products were examined by X-ray diffraction (XRD), scanning electron microscopy (SEM-6301F), high resolution transmission electron microscopy (HRTEM-JEM2011), energy dispersive spectroscopy (EDS) and X-ray photo-spectroscopy (XPS). Photoluminescence (PL) measurement was conducted at room temperature using the 325 nm line of the He–Cd laser which was used as the excitation source. The electrochemical measurements were performed on a CHI660C electrochemical workstation with a conventional three-electrode configuration. A modified electrode (3 mm in diameter) was used as the working electrode. Platinum was used as the counter electrode with Hg/Hg_2SO_4 as the reference electrode. All measurements were carried out in a 0.1 M phosphate buffer solution (PBS, pH 6.9) at room temperature (25 °C).

2.4. Fabrication of the modified glassy carbon electrode

The GC electrode was successively polished to a mirror followed by a thorough rinse with doubly distilled water and modified with elbow shaped SZO NWs. To prepare the working electrode, 10 mg of sample (each case) was dispersed in 900 μL isopropanol + 100 μL Nafion solutions (5 wt%) and then ultrasonically dispersed for 15 min to form a uniform suspension. Then, 1.0 μL of the suspension was dropped onto a GC electrode to form a uniform layer and dried at 60 °C for 20 min. For comparison, the ZnO/GC electrode was also prepared with the same procedure.

3. Results and discussions

3.1. Material characterization

Fig. 1 shows the XRD spectra, in which all the diffraction peaks can be assigned to those of a ZnO wurtzite crystal structure. The presence of Zn peaks in the pattern reveals that a small amount of Zn powder remains phase separated during the experiment. There is no trace of any crystalline secondary phase, which verifies the substitution of Sb into the ZnO lattice. A close view in the range $2\theta = 31–37°$ illustrates that the peaks are slightly shifted towards the smaller angles, as compared with undoped, as clearly shown in the inset. The doped Sb does not alter the crystal structure but it causes a slight c-axis lattice expansion at about 0.014 nm. The increase in lattice constants is due to the difference in ionic radii, as the ionic radius of the Sb^{3+} (0.078nm) dopant is larger than that of the Zn^{2+} (0.074nm). This change in the lattice constants confirms the successful substitution of Sb atoms into the ZnO lattice.

Fig. 2(a) shows the SEM morphology of the un-doped sample and consists of sunflower shapes composed of vertically straight nanowires with a uniform diameter in the range of 50–200 nm. Fig. 2(b) shows the morphology of the Sb-doped sample and consists of elbow shaped nanowires with lengths up to several hundreds of micrometres and thickness of about 20 nm. The differences in morphology of the doped and undoped NWs are due to the change in surface free energy which determines the growth conditions necessary for nucleation. Fig. 2(c) shows the EDS of the Sb-doped sample from the area indicated in Fig. 2(b). The spectrum consists of Zn, O and Sb peaks which confirms the presence of Sb in the sample. The detailed microstructure and composition of the product are characterized using HRTEM, selected-area electron diffraction (SAED), and EDS. Fig. 2(d) shows the bright-field TEM image of the un-doped NWs. Fig. 2(e) is the TEM image of a single elbow with a left and right side of 80 and 50 nm in width, respectively. The angle at the kinks has a little variation from 54–60° (see Fig. 2e). The *in situ* EDS elemental analysis from the arrow indicated in Fig. 2(e) is shown in Fig. 2(f). The spectrum consists of only Zn, O and Sb (the Cu signal comes from the TEM grid). The presence of Sb confirms the existence of Sb in the elbow shaped NW.

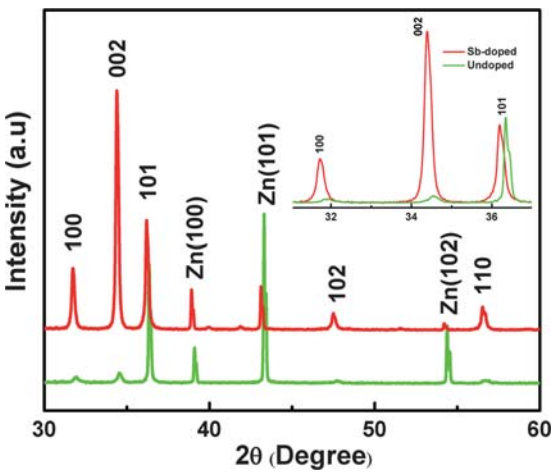

Fig. 1 XRD patterns of the un-doped and doped sample.

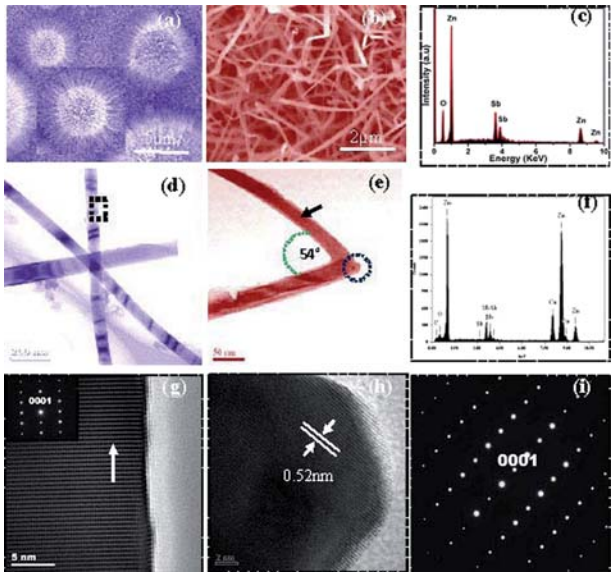

Fig. 2 FESEM images of (a) un-doped ZnO NWs (b) Sb-doped elbow shaped ZnO NWs (c) EDS image of doped NWs (d) TEM image of un-doped (e) TEM of elbow shaped Sb-doped ZnO NW (f) EDS image of doped NWs (g) HRTEM image of un-doped, inset is the corresponding SAED (h) HRTEM image of Sb-doped (i) SAED of doped NWs.

Quantitative analysis reveals that the average amount of Sb content is about 2% in each of the elbows. Statistical analysis of the EDS measurements over a dozen of the elbow NWs demonstrates that the variation of Sb is rather small and the composition of the Sb dopant is uniform throughout the specimen. Therefore, the EDS results further demonstrate that Sb is incorporated into the elbow shaped ZnO, which is also in good agreement with the XRD results. The HRTEM image of the un-doped NW from the doted rectangular area indicated in (Fig. 2(d)) is shown in Fig. 2(g) along with the SAED (inset) and shows the single crystalline wurtzite structure along [0001]. The HRTEM image of the elbow shaped SZO NW taken from the doted circle area indicated in Fig. 2(e) is shown in Fig. 2(h) and found to be single crystalline. HRTEM images show that both segments grow along the [0001] direction and the atomic structure is coherent at the kinks. The corresponding SAED pattern is found to be identical along the entire part of the elbow as shown in Fig. 2(i). Both nanostructures are grown *via* the vapor–solid (VS) mechanism. The growth mechanism of the NWs is not fully understood at the moment. However, we propose that the Sb plays a significant role in defining the structure of the elbow shaped NWs *via* influencing the nucleation at the growth front. It is possible to obtain [0001]-axial undoped and elbow shapes Sb doped NWs using similar conditions but a different source type.

The valence state of the Sb element has been analyzed by XPS. Fig. 3 shows the XPS survey along with the Sb 3d peak in the inset. The Sb-doped sample shows that the Sb peaks including O1s are located at 530.6 and 540 eV, corresponding to the electronic states of Sb $3d_{5/2}$ and Sb $3d_{3/2}$ respectively. The Sb $3d_{3/2}$ peak in the spectrum clearly indicates that the Sb element has been doped into elbow shaped NWs. The XPS results are also in good agreement with our previous work.[31]

Fig. 4(b) shows the room temperature PL spectra of un-doped and doped NWs. The un-doped NWs consist of a strong UV

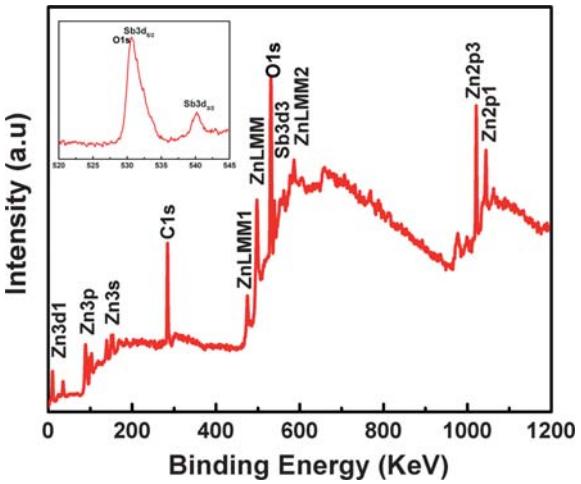

Fig. 3 XPS survey spectrum of Sb-doped ZnO nanowires. Inset; XPS spectrum corresponding to the Sb 3d peak.

band peak at 376 nm and a weak broad green band centred at about 550 nm. As compared with undoped NWs, the doped NWs exhibit three major changes in the spectrum which makes it interesting for the discussion. Firstly, a large red shift of 10 nm in UV emission, secondly, an increase in the green emission band (which usually corresponds to deep-level defect transitions) and the decrease in the intensity of UV emission. The red shift in UV, in other words, the narrowing in the band gap with Sb doping may be due to the strong sp-d exchange interactions between the band electrons of ZnO and the localized "d" electrons of Sb^{3+} ions, which form band impurity states near the bottom of the conduction band (see ref. 28). The merging of these impurity states with the bottom of the conduction band may give rise to the narrowing of the band gap. The origin of the green emission band in the ZnO band gap has been studied intensively and is considered to be due to the singly ionized oxygen vacancies, resulting from the recombination of a photogenerated hole with a singly ionized charge state.[32] The decrease in the intensity of UV emission may indicate that the amount of defects (like Zn interstitials) increases, probably due to the incorporation of Sb

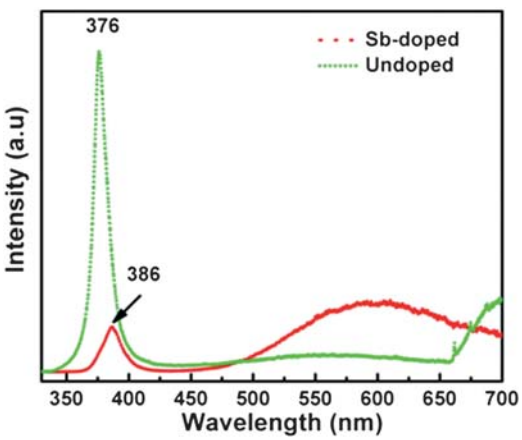

Fig. 4 Room temperature PL spectra of un-doped and Sb-doped ZnO nanowires.

ions into the lattices of ZnO (because of relative ionic radii, the Sb ions replace the Zn ions in the lattices).[33] Previously many researchers have demonstrated that the defects play a very important role in the electrochemical properties of materials.[34]

3.2. Electrochemical measurements

3.2.1. Cyclic voltammograms. Electrochemical oxidation of L-CySH on bare GC, ZnO/GC and SZO/GC electrodes are investigated by cyclic voltammetry in the potential range of −0.1 to +0.8 V *versus* Hg/Hg_2SO_4 at a scan rate of 20 mV s^{-1}. Typical cyclic voltammograms (CV) of the three electrodes in 0.1 M PB solution with 20 μM L-CySH are shown as A, B and C in Fig. 5. These CVs are in good agreement with the results reported previously.[3,35] The background current of the SZO/GC electrode is higher than that of the GC and ZnO/GC electrodes. This is due to the rough surface of the elbow shaped ZnO NWs caused by Sb doping. The oxidation peak potential of L-CySH can be observed at Ep ~ +0.19 V using the SZO/GC electrode and is lower than that of the GC and ZnO/GC (at Ep ~ +0.23) electrodes. The oxidation peak current of L-CySH using the SZO/GC modified electrode is much higher than that of the GC and ZnO/GC electrodes. This implies that the oxidation of L-CySH at the SZO/GC electrode is significantly improved. This improvement can be ascribed to the superior electrochemical properties of the SZO/GC electrode, which may result in increased amount of defects in Sb-doped NWs. Based on this, it is expected that sensitive electrodetection of L-CySH can be achieved using the SZO/GC electrode. Upon reverse sweep, no reduction waves of L-CySH are observed using the above electrodes in the potential range studied. This can be attributed to the incorporation of Sb into ZnO elbow shaped NWs which led to enhanced electrocatalytic ability of the modified electrode. The effect of the scan rate on the cyclic voltammetric performance during L-CySH oxidation at the SZO/GC electrode is also investigated. As shown in inset Fig. 5, the peak current increases linearly with the square root of the scan rate.

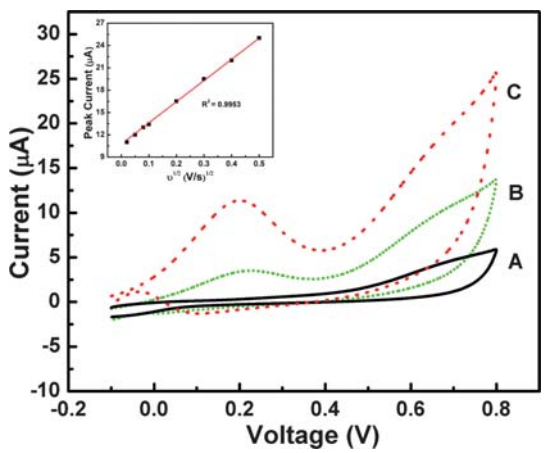

Fig. 5 Cyclic voltammograms of the bare GC (A), ZnO/GC (B) and SZO/GC (C) electrodes in the presence of 20 μM L-CySH in 0.1 M PBS, pH 6.9 at a scan rate of 20 mV s^{-1}. Inset is the plot of peak current against the square root of the scan rate for L-CySH oxidation at the SZO/GC electrode.

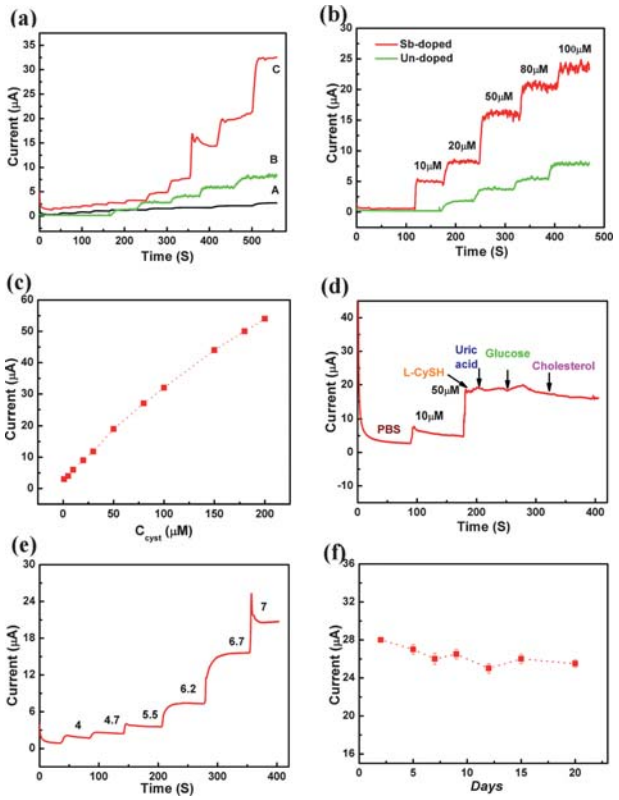

Fig. 6 The amperometric response of the bare GC, ZnO/GC and SZO/GC electrodes at +0.5 V in stirred 0.1 M PBS with successive addition of 20 μM L-CySH. (b) Amperometric response to different concentrations of L-CySH obtained at the ZnO/GC and elbow SZO/GC electrodes. (c) Calibration curve of the current response to the different concentration of L-CySH at the SZO/GC electrode in 0.1 M PBS. (d) The effect of interfering species on the response of the SZO/GC electrode. (e) A plot of oxidation peak current of L-CySH at the modified electrode at different pH values. (f) The long-term stability of the modified electrode.

This finding indicates that the oxidation reaction is a diffusion-controlled process.

3.2.2. Amperometric response. The typical amperometric responses of the three modified electrodes to the successive addition of 10 μM L-CySH at +0.5 V *versus* Hg/Hg_2SO_4 are shown in Fig. 6(a). In comparison with the bare GC and ZnO/GC modified electrodes, the SZO/GC modified electrode exhibits a rapid and sensitive response to the change of L-CySH and an obvious increase in current as clearly observed as "C" in Fig. 6(a). The modified electrode achieved 95% steady state current within less than 6s. This indicates good electrocatalytic, oxidative and fast electron exchange behavior of the modified electrode. The amperometric responses of the two modified electrodes are also examined in response to different concentrations of L-CySH. The corresponding results are shown in Fig. 6(b). It is clear that the SZO/GC electrode displays an amplified current response compared to the ZnO/GC electrode (about five times higher than that of the ZnO/GC electrode). These results are consistent with those in Fig. 6(a). The corresponding calibration plot for L-CySH detection at the SZO/GC modified electrode is investigated under optimum experimental conditions. Following the increase of the L-CySH

concentration, the response current increases linearly as shown in Fig. 6(c). The linear range of the calibration curve is from 0.075 to 100 μM (correction coefficient $R = 0.9953$) with a sensitivity of 400 nA μM^{-1} and a limit of detection (LOD) about 0.025 μM. These findings indicate that the SZO/GC electrode is more sensitive for the detection of L-CySH than those reported in the literature.[3,35–37] The performance of the biosensor based on SZO NWs proves that the modified electrode is very sensitive to the L-CySH and demonstrates that the Sb doping improves the electrochemical property of ZnO and enhances the electrode activity for L-CySH determination due to providing a higher surface area, enhanced electrostatic interaction, a compatible microenvironment and introducing more edge plane sites on the surface.

3.2.3. Interference. The electrocatalytic behavior of the modified electrodes is also investigated for practical use, by introducing electroactive bio-species such as uric acid, glucose, cholesterol and hydrogen peroxide. These species are consecutively added into continuously stirred 0.1 M PB solution. The influence of the above species on the detection of L-CySH at the modified electrode is shown in Fig. 6(d). It can be observed that glucose causes a small current increment of about 3% compared with 50 μM L-CySH, while uric acid has no significant influence on the modified electrode. However a decrease in current of about 5% by the addition of cholesterol is observed as shown in Fig. 6(d). These results indicate that modified electrode has good anti-interference ability.

3.2.4. Determination of L-Cysteine in real samples. In order to demonstrate the electrocatalytic oxidation of L-cysteine in real samples, we examined this ability in the voltammetric determination (not shown) of L-CySH in some samples, such as the human blood serum and acetylcysteine tablets purchased from commercial sources. The determination of L-cysteine in these samples was carried out by the standard addition method in order to prevent any matrix effect. The total concentration of L-CySH in patient human blood serum was found to be $1.37 \pm 0.4 \times 10^{-4}$ M by the present electrode which is in good agreement with the real value ($1.48 \pm 0.34 \times 10^{-4}$ M in serum of human blood).[38] Also the total concentration of L-CySH in the acetylcysteine sample was found to be $(4.95 \pm 0.03) \times 10^{-3}$ M as compared with the data reported in previous works (5.09×10^{-3} M).[39] These results suggest that the proposed electrode is very reliable and sensitive with regard to determining L-CySH.

3.2.5. pH response. The activity of the modified electrode is also affected by the pH of the PB solution, therefore the pH effect on the modified electrode performance is also investigated by measuring the current response to 10 μM L-CySH. The electrochemical oxidation of L-CySH on a solid electrode may proceed by the following mechanism (see ref. 14).

$$\text{L-CySH} \rightarrow \text{L-CyS}^- + \text{H}^+ \quad (1)$$

$$\text{L-CyS}^- \rightarrow \text{L-CyS*ads} + \text{e}^- \quad (2)$$

$$2\text{L-CyS*ads} \rightarrow \text{L-CySSCy} \quad (3)$$

The variations in the current response at the different pH values are analyzed. ZnO is a kind of amphoteric compound and not stable in both strong acid and base solutions, therefore, considering this and the physiological conditions, the pH dependence of the sensor is evaluated in a range of pH. As clearly seen in Fig. 6(e) the sensor shows an optimal sensitivity of response at pH 7 corresponding to a series of pH values.

3.2.6. Stability. The long-term storage stability of the SZO/GC electrode is also investigated and the results are shown in Fig. 6(f). It can be observed that the electrocatalytic property of the modified electrode to CySH oxidation remains satisfactory; only 5% current loss after 4 days and 15% current loss after 20 days are observed. The performance of the modified electrode for L-CySH detection is compared with those of previously reported electrodes. It is clear from Table 1 that the presented electrode exhibited an excellent performance.

4. Conclusions

In this manuscript, an elbow shaped SZO NWs based L-cysteine biosensor has been successfully fabricated. The synthesized elbow shaped SZO NWs exhibit an increased amount of deep-level defect transitions in their visible luminescence which leads to a significant role in the determination of L-CySH using a SZO/GC electrode. The electrochemical studies show that the oxidation of L-CySH is catalyzed at pH 6.9 and a reduction in peak potential at the surface of the SZO/GC electrode. The modified electrode shows excellent electrochemical properties, such as high reproducible sensitivity, a low limit of detection, favorable stability and a resistance to interference. To the best of our knowledge, this is the first time such a very high-sensitivity has been achieved for L-CySH by using a SZO/GC modified electrode. In addition, it has been revealed that Sb doping improves the electrochemical properties of the ZnO, which in turn enhances the sensitivity of the electrode for L-CySH detection. Furthermore, it has been found that the proposed electrode facilitates the low potential amperometric detection of L-CySH as compared to the previously

Table 1 A comparison of the performance of some modified electrodes used in the electrocatalysis of L-cysteine

Electrode materials	Sensitivity/nA μM^{-1}	Dynamic Linear range/μM	Peak potential (Ep)/V	Appl. Potential (Volts)	LOD/μM	Ref.
BCNT/GCE	25.3 ± 1.2	0.02–0.78	0.47	0.0 to 1.0	0.26	[36]
MCNT/GCE	3.0	10–500	0.18	———	5.4	[37]
Pt/CNT electrode	———	0.5–100	0.46	−0.5 to 0.7	0.3	[3]
ZnO Nanoparticles/GCE	28.5	0.3–20	0.5	0.0 to 0.65	0.05	[35]
Sb-ZnO/GCE	400	0.075–100	0.19	−0.1 to 0.8	0.025	Present work

reported electrodes. These characteristics demonstrate that the SZO/GC electrode should be suitable for the determination of L-CySH in biological systems. Thus a SZO/GC electrode could provide a new platform for the electroanalysis of thiols.

Acknowledgements

This work is financially supported by the National 973 Project of China and the Chinese National Nature Science Foundation. This work made use of the resources of the Beijing National Center for Electron Microscopy. The authors are also grateful to the Higher Education Commission (HEC) and PINSTECH (PAEC) Pakistan for the financial support to Mashkoor Ahmad.

References

1 M. L. Huang and D. M. Stanbury, *Inorg. Chem.*, 2005, **44**, 3541.
2 A. K. M. Kafi, F. Yin, H.-K. Shin and Y.-S. Kwon, *Curr. Appl. Phys.*, 2007, **7**, 496.
3 S. D. Fei, J. H. Chen, S. Z. Yao, G. H. Deng, D. L. He and Y. F. Kuang, *Anal. Biochem.*, 2005, **339**, 29.
4 S. A. Wring, J. P. Hart and B. J. Birch, *Analyst*, 1989, **114**, 1563.
5 J. Kulys and A. Drungiliene, *Anal. Chim. Acta*, 1991, **243**, 287.
6 P. C. White, N. S. Lawrence, J. Davis and R. G. Compton, *Anal. Chim. Acta*, 2001, **447**, 1.
7 N. Maleki, A. Safavi, F. Sedaghati and F. Tajabadi, *Anal. Biochem.*, 2007, **369**, 149.
8 J. Dumonceaux, C. Goujon, V. Joliot, P. Briand and U. Hazan, *J. Virol.*, 2001, **75**, 5425.
9 P. Schrynemackers-Pitance and S. Schoos-Berbette, *Clin. Chim. Acta*, 1987, **166**, 91.
10 J. A. Reyanud, B. Maltoy and P. Canessan, *J. Electroanal. Chem.*, 1980, **114**, 195.
11 D. L. Rabenstein and G. T. Yamashita, *Anal. Biochem.*, 1989, **180**, 259.
12 J. L. D'Eramo, A. E. Finkelstein, F. Q. Boccazzi and O. Fridman, *J. Chromatogr., B: Biomed. Sci. Appl.*, 1998, **720**, 205.
13 P. J. Vandeberg and D. C. Johnson, *Anal. Chem.*, 1993, **65**, 2713.
14 T. R. Ralph, M. L. Hitchman, J. P. Millington and F. C. Walsh, *J. Electroanal. Chem.*, 1994, **375**, 1.
15 M. T. Stankovich and A. J. Bard, *J. Electroanal. Chem.*, 1977, **75**, 487.
16 F. G. Banica, J. C. Moreira and A. G. Fogg, *Analyst*, 1994, **119**, 309.
17 D. Mimica, F. Bedioui and J. H. Zagal, *Electrochim. Acta*, 2002, **48**, 323.
18 K. P. Gong, X. Z. Zhu, R. Zhao, S. X. Xiong, L. Q. Mao and C. F. Chen, *Anal. Chem.*, 2005, **77**, 8158.
19 N. Sehlothl, T. Nyokong, J. H. Zagal and F. Bedioui, *Electrochim. Acta*, 2006, **51**, 5125.
20 I. Willner, *Science*, 2002, **298**, 2407.
21 X. Zhu, I. Yuri, X. Gan, I. Suzuki and G. Li, *Biosens. Bioelectron.*, 2007, **22**, 1600.
22 Z. Y. Fan and J. G. Lu, *Appl. Phys. Lett.*, 2005, **86**, 123510.
23 S. Kumar, V. Gupta and K. Sreenivas, *Nanotechnology*, 2005, **16**, 1167.
24 J. X. Wang, X. W. Sun, A. Wei, Y. Lei, X. P. Cai, C. M. Li and Z. L. Dong, *Appl. Phys. Lett.*, 2006, **88**, 233106.
25 S. Krishnamurthy, T. Bei, E. Zoumakis, G. P. Chrousos and A. Iliadis, *Biosens. Bioelectron.*, 2006, **22**, 707.
26 A. Wei, X. W. Sun, J. X. Wang, Y. Lei, X. P. Cai, C. M. Li, Z. L. Dong and W. Huang, *Appl. Phys. Lett.*, 2006, **89**, 123902.
27 M. Ahmad, J. Zhao, J. Iqbal, W. Miao, L. Xie, R. Mo and J. Zhu, *J. Phys. D: Appl. Phys.*, 2009, **42**, 165406.
28 W. Guo, A. Allenic, Y. B. Chen, X. Q. Pan, Y. Che, Z. D. Hu and B. Liu, *Appl. Phys. Lett.*, 2007, **90**, 242108.
29 V. Urbanova, K. Vytras and A. Kuhn, *Electrochem. Commun.*, 2010, **12**, 114.
30 C. Y. Deng, J. H. Chen, X. L. Chen, C. H. Xiao, L. H. Nie and S. Z. Yao, *Biosens. Bioelectron.*, 2008, **23**, 1272.
31 M. Ahmad, R. Din, C. Pan and J. Zhu, *J. Phys. Chem. C*, 2010, **114**(6), 2560.
32 M. W. Ahn, K. S. Park, J. H. Heo, J. G. Park, D. W. Kim, K. J. I. Choi, J. H. Lee and S. H. Hong, *Appl. Phys. Lett.*, 2008, **93**, 263103.
33 S. H. Kim, A. Umar, Y. K. Park, J.-H. Kim, E. W. Lee and Y. B. Hahn, *J. Alloys Compd.*, 2009, **479**, 290.
34 M. Ahmad, C. Pan, J. Iqbal, L. Gan and J. Zhu, *Chem. Phys. Lett.*, 2009, **480**, 105.
35 R. Hallaj, A. Salimi, K. Akhtari, S. Soltanian and H. Mamkhezri, *Sens. Actuators, B*, 2009, **135**, 632.
36 C. Deng, J. Chen, X. Chen, M. Wang, Z. Nie and S. Yao, *Electrochim. Acta*, 2009, **54**, 3298.
37 A. Salimi and R. Hallaj, *Talanta*, 2005, **66**, 967.
38 http://en.wikipedia.org/wiki/list_of human blood_components.
39 J.-B. Raoof, R. Ojani, H. Beitollahi and R. Hossein Zadeh, *Anal. Sci.*, 2006, **22**, 1213.

